# History – matching flow simulations and time-lapse seismic data from the Sleipner $CO_2$ plume

R.A. Chadwick* & D. J. Noy

British Geological Survey, Keyworth, Nottingham, NG12 5GG, UK,

*Corresponding author: R.A. Chadwick, e-mail: rach@bgs.ac.uk

**Abstract**
Since its inception in 1996, the $CO_2$ injection operation at Sleipner has been monitored by 3D time-lapse seismic surveys. Striking images of the $CO_2$ plume have been obtained showing a multi-tier feature of high reflectivity. In the medium to longer term, the topmost layer of $CO_2$, accumulating and migrating directly beneath the topseal is the main determinant of storage site performance. Fortunately it is this topmost layer that can be most accurately characterized, its rate of growth quantified, and $CO_2$ flux arriving at the reservoir top estimated. The latter is mostly controlled by pathway flow through thin intra-reservoir mudstones. This has increased steadily with time suggesting either that pathway transmissivities are increasing with time, and/or the pathways are becoming more numerous. Detailed 3D history-matching of the topmost layer cannot easily match the observed rate of spreading. Isotropic permeabilities result in a stronger radial component than observed and a degree of anisotropic permeability, higher in a N-S direction, is possible. The main contributor to the mismatch however is likely to be small but significant uncertainty in the depth conversion. Irrespective of uncertainty, the observed rate of lateral migration seems to require very high permeabilities, and is, moreover, suggestive of a topseal which behaves like a 'hard' impermeable flow barrier. Detailed studies such as this will provide important constraints on longer-term predictive models of plume evolution and storage performance which are key regulatory requirements.

**Keywords:** Sleipner, Utsira Sand, $CO_2$ plume, seismic monitoring, time-lapse seismic, reservoir flow simulation, history-matching

Large-scale underground storage of industrially-produced carbon-dioxide has the potential to play a key role in reducing man-made emissions of greenhouse gases (IPCC 2005). The $CO_2$ injection operation at Sleipner, in the central North Sea between the UK and Norway, commenced in 1996 and is the world's longest-running industrial-scale storage project. It is also, so far, the only example of underground $CO_2$ storage arising as a direct response to environmental legislation (Baklid et al. 1996).

$CO_2$ separated from natural gas produced at Sleipner is injected into the Utsira Sand, a major saline aquifer of late Cenozoic age (Fig. 1a). Well logs (Fig. 1b) show the Utsira Sand to have a sharply-defined top and base, and gamma-ray values typically around 25 API units compared to 90 API units in the overlying caprock. Gamma-ray

and resistivity peaks within the sand are interpreted as thin intra-reservoir mudstones, mostly around 1m thick (Zweigel et al. 2004).

The injection point is at a depth of about 1012 m below sea level, some 200 m below the reservoir top, with around twelve million tonnes (Mt) of $CO_2$ currently stored. A comprehensive monitoring programme has been carried out, with multiple time-lapse 3D seismic surveys, augmented by high resolution 2D seismic, seabottom gravity, controlled-source electromagnetic and seabed imaging surveys. This paper describes analysis of the time-lapse 3D seismic datasets acquired up to 2006, comprising the 1994 (baseline), 1999 (cumulative 2.35 Mt of $CO_2$ injected), 2001 (cumulative 4.26 Mt injected), 2002 (cumulative 4.97 Mt injected), 2004 (cumulative 6.84 Mt injected) and 2006 (cumulative 8.4 Mt injected) surveys.

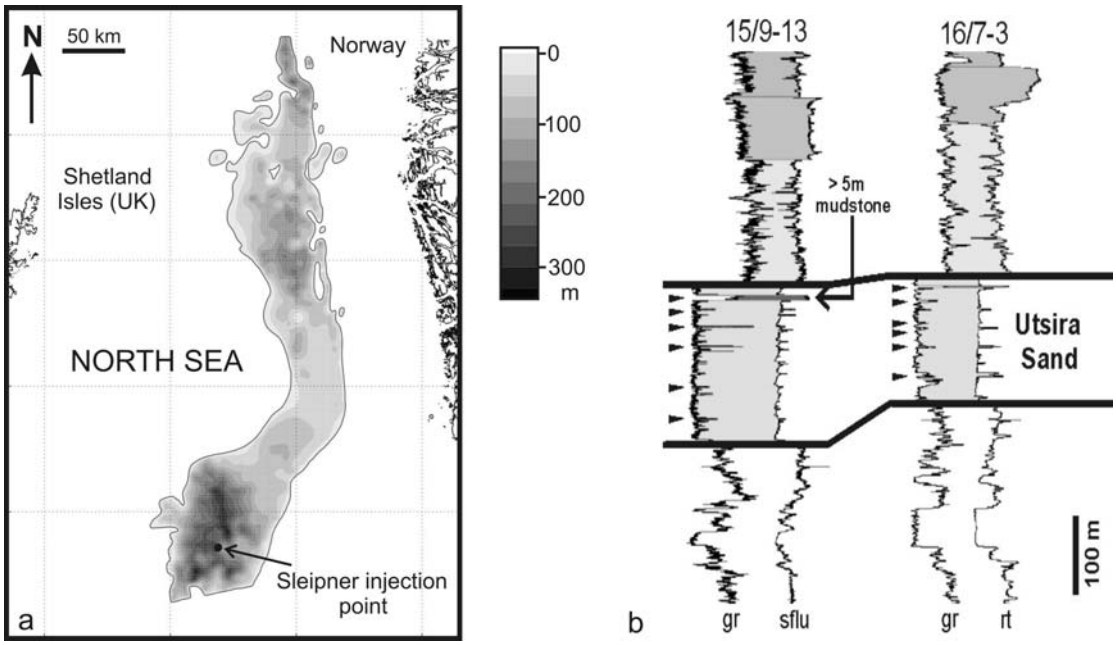


***Figure 1*** *a) Location of the Sleipner injection operation showing the Utsira Sand with thicknesses b) Geophysical logs through the Utsira Sand showing gamma-ray and resistivity peaks corresponding to thin intra-reservoir mudstones. Note thicker (> 5m) mudstone near reservoir top. Wells 15/9-13 and 16/7-3 lie around 1 km WSW and 12 km ENE of the injection point respectively. Log types: gr = gamma ray; rt = deep resistivity; sflu = spherical-focussed resistivity.*

The time-lapse seismic data clearly image the progressive development of the $CO_2$ plume, around 200 m in height and elliptical in plan view (Fig. 2). By 2006 the NNE-trending long axis of the plume spanned 3.6 km with a short axis of around 1 km. The plume forms a prominent multi-tier feature comprising a number of bright sub-horizontal reflections, interpreted as arising from discrete layers of $CO_2$, each up to a few metres thick, and mostly accumulating beneath the intra-reservoir mudstones (Fig. 1b). The $CO_2$ layers formed early in plume evolution (by 1999) and have remained identifiable ever since. The upper layers continue to spread laterally and generally increase in brightness, whereas the lower layers have stabilised in size and are growing progressively dimmer. Vertical linear features within the plume characterized by reduced reflection amplitudes and localized velocity pushdown are

interpreted as ‘chimneys’ of moderate or high $CO_2$ saturation (Chadwick et al. 2004). The most prominent of these is located roughly above the injection point (Fig. 2), and is interpreted as the main conduit for $CO_2$ upward transport through the reservoir and the main feeder of the laterally spreading thin layers. Within the reservoir overburden, there is no evidence of systematic changes in seismic signature, indicating that $CO_2$ is being contained within the storage reservoir.

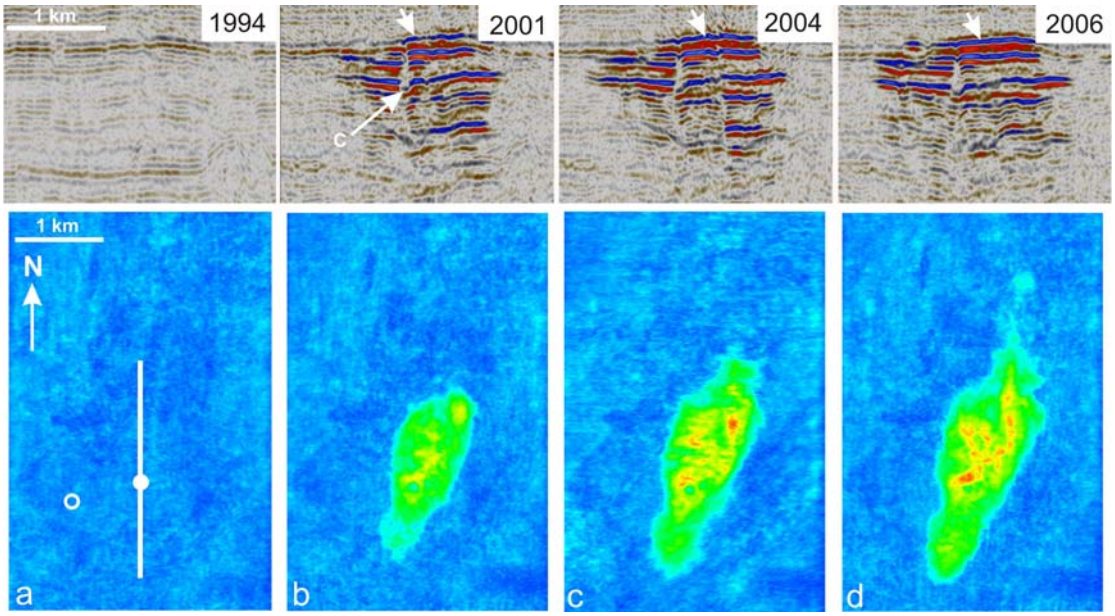


***Figure 2*** *Seismic images of the Sleipner plume showing its development from 1994 (pre-injection) through to 2006. Top panels show a N-S seismic section through the plume, bottom panels show plan views of the plume displayed as total reflection amplitude. C (on 2001 section) denotes the main feeder chimney in the plume. White arrow denotes topmost $CO_2$ layer. Location of N-S seismic section, injection point (filled circle) and well 15/9-13 (open circle) also shown.*

Quantitative analysis (Chadwick et al. 2004, 2005) has shown that while the seismic images are consistent with the known injected amounts of $CO_2$, they do not provide a unique verification of injected mass. Significant uncertainties remain, particularly regarding seismic properties of $CO_2$-saturated rock, and the fine-scale distribution of dispersed $CO_2$ in between the reflective layers. Similarly, reservoir flow simulations (Lindeberg et al. 2001; Chadwick et al. 2008) have reproduced the current observed development of the $CO_2$ plume as a multi-tier layered structure. However because the structural geometry of the sealing intra-reservoir mudstones is not precisely known, simulated layer thicknesses are not tightly constrained and have not yet been robustly matched to thicknesses obtained directly from the seismic data.

The objective of this paper is to look at key aspects of the seismic data that constrain models of $CO_2$ migration through the reservoir, and to assess whether flow processes in the reservoir are understood to the extent that predictions and simulations of future, longer-term, plume behaviour are likely to be robust.

## Analysis of the topmost $CO_2$ layer

Although up to nine individual $CO_2$ layers have been identified in the plume (Chadwick et al. 2004), from the viewpoint of determining medium to long term storage site performance, understanding the topmost layer is of paramount importance. Long-term flow simulations of the Sleipner plume (Erik Lindeberg pers. comm.) show that within a few decades of ceasing injection most of the $CO_2$ will have migrated to the top of the reservoir as a buoyant fluid phase. Here, trapped beneath the undulating caprock, it will migrate laterally over significant distances. Over the succeeding centuries, dissolution of $CO_2$ at the base of the migrating layer, and convective sinking of $CO_2$ in solution, will gradually 'erode' the $CO_2$ layer and progressively reduce its mobility. Ultimately, after a few thousand years, most of the $CO_2$ will be fixed in a gravitationally stable dissolved form. Risk assessment therefore requires robust prediction of how the $CO_2$ will migrate in the free phase for a protracted period after site closure.

Fortunately, of all the layers in the plume, the topmost is imaged most clearly by the time-lapse monitoring data. Currently its lateral spread can be tracked in detail and its progressive increase in thickness and volume quantified with a degree of accuracy. The latter parameter allows the total upward flux of $CO_2$ through the reservoir to be calculated, which provides insights into reservoir flow behaviour and how this changes with time.

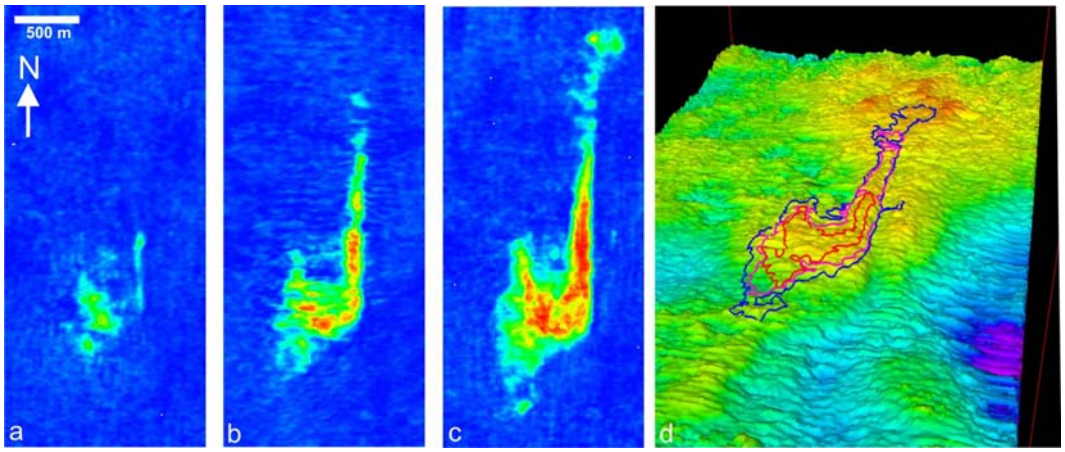


***Figure 3*** *Growth of the topmost $CO_2$ layer mapped as amplitude changes at the top of the Utsira Sand a) 2001 minus 1994 difference b) 2004 minus 1994 difference c) 2006 minus 1994 difference d) 3D view (looking north) of the top Utsira Sand surface (mapped on the baseline 1994 dataset) showing the $CO_2$ - water contacts in 2001 (red), 2004 (purple) and 2006 (blue). RMS amplitudes were extracted from a 4 ms window centred on the trough event corresponding to the negative acoustic impedance change at the top of the $CO_2$ layer.*

Quantitative analysis of the 2006 time-lapse processing ensemble, comprising the 1994, 2001, 2004 and 2006 surveys, forms the basis of this paper. Reflection amplitude changes at the top of the Utsira Sand correspond to the development of the topmost $CO_2$ layer and show how it has grown through time (Fig. 3). A north-trending linear prolongation of the layer is particularly prominent and corresponds to $CO_2$ migrating northwards along a linear ridge at the reservoir top (Fig. 3d). The $CO_2$-

water contacts correspond to the outer edges of the $CO_2$ layers, defined as the outer limit of detectable amplitude change.

Amplitude maps of the topmost layer from the full time-lapse dataset (Fig. 4) show how $CO_2$ first reached the reservoir top in 1999 (just prior to the first time-lapse repeat survey), as two small separate accumulations. By 2001 these had coalesced into a single accumulation which continued to expand thereafter.

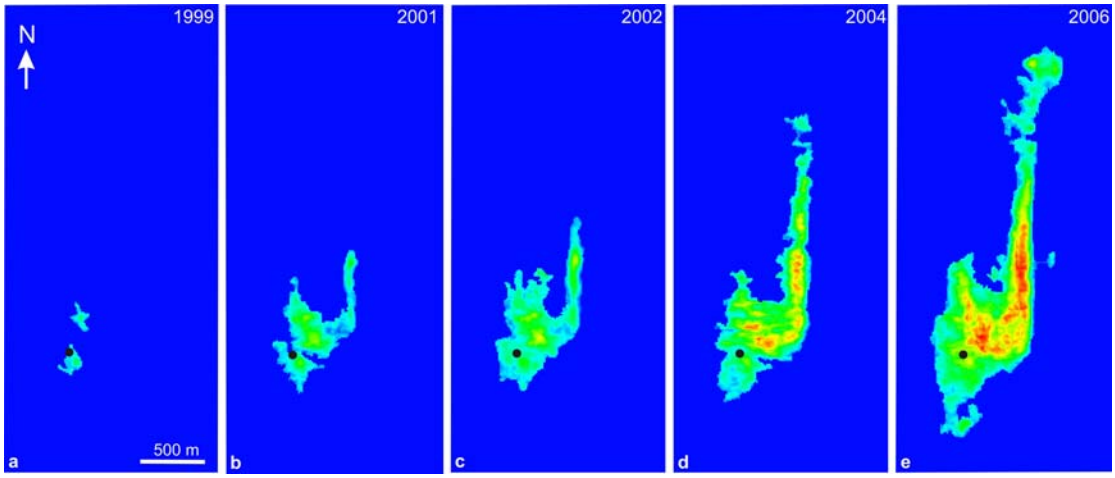


***Figure 4*** *Amplitude maps of the topmost layer through time. Black spot denotes the location of the injection point for reference. (Note however that the injection point lies roughly 200 m beneath the topmost layer so does not directly control its growth).*

***Layer thicknesses from seismic amplitudes***

Earlier work (Arts et al. 2003, Chadwick et al. 2005) has shown that layer reflectivity, for the most part follows a thin-layer tuning relationship, with reflection amplitudes directly related to layer thicknesses. Rock physics properties were calculated for a range of $CO_2$ saturations in the Utsira Sand using the Gassman fluid substitution equation (Mavko et al. 2003), calibrated by p and s-wave velocity and density data from well logs (Figure 5a). For uniform fluid mixing (likely in the high saturation $CO_2$ layers), substitution of water by $CO_2$ reduces $V_p$ from 2050 $ms^{-1}$ to around 1420 $ms^{-1}$ for $CO_2$ saturations above 0.2. A synthetic wedge model was constructed using the calculated seismic properties and from this an amplitude – thickness relationship was derived (Fig. 5b). The amplitude-thickness relationship for the observed data was then obtained by scaling the maximum tuning amplitude of the synthetic data to the maximum seismic amplitudes observed in the plume. Two simplifying assumptions were made in this analysis. Firstly the $CO_2$ wedge model was incorporated a uniformly high $CO_2$ saturation. In terms of the calculated seismic response this is very reasonable given the characteristic Gassman fluid response with rapid velocity decrease even at low $CO_2$ saturations and the fact that low $CO_2$ saturations are likely to be restricted to the very lowermost part of the layer (Fig. 5c). Secondly, rock properties were assumed to be laterally uniform. This is also reasonable given the absence of data to the contrary and the very large changes induced by the $CO_2$ compared to likely lithological effects.

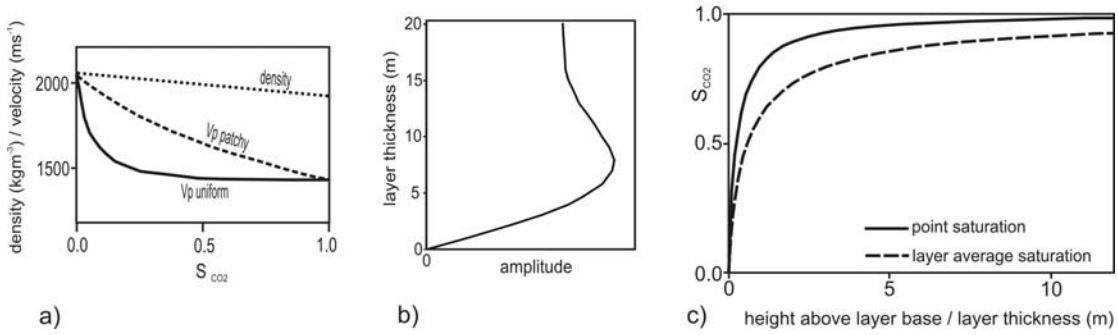


***Figure 5*** *a) variation of seismic velocity in the Utsira Sand with $CO_2$ saturation, calculated for uniform (Reuss bound) and patchy (Hills bound) fluid mixing b) amplitude – thickness relationship from a synthetic wedge model of a $CO_2$-saturated layer within water saturated sand c) layer thickness- saturation function based on capillary pressure data from Utsira core.*

The amplitude - thickness relationship was used to transform observed amplitudes to layer thicknesses (Fig. 6a - c). $CO_2$ saturations within the layer were calculated from a capillary pressure - saturation relationship determined by centrifuge experiments on core material from the Utsira Sand (Erik Lindeberg pers. comm.). The capillary pressure, $p_c$, between the formation brine and the injected $CO_2$ will cause the $CO_2$ saturation, $S_{CO2}$, to vary with height, $h$, in each $CO_2$ layer. The gradient can be computed by balancing the buoyancy, $\Delta\rho \cdot g \cdot h$, with the capillary pressure.

In SI units:

$$\Delta\rho \cdot g \cdot h = p_c = 810.35(1- S_{CO2})^{-0.948} \qquad \text{Equation 1}$$

The variation of $S_{CO2}$ with $h$ was thereby computed and also the average value of $S_{CO2}$ for a range of layer thicknesses (Fig. 5c). This relationship was used to compute average saturations for the topmost layer (Fig. 6 d-e).

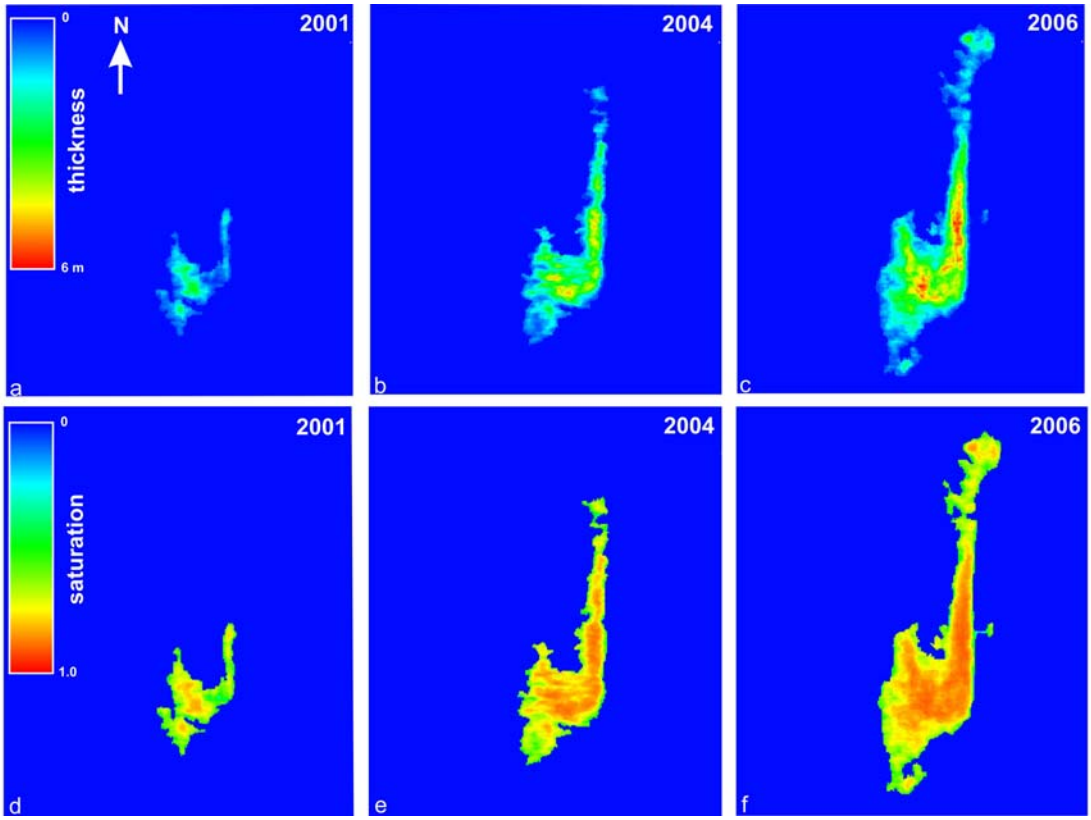


***Figure 6*** *Topmost $CO_2$ layer properties a-c) thicknesses derived from reflection amplitudes d-f) average saturations determined from capillary pressure data.*

***Layer thicknesses from structural analysis***

An alternative, wholly independent way of obtaining layer thicknesses is by topographic analysis of the reservoir top (Fig. 7). In map view (Figure 3d), the outer limit of $CO_2$ reflectivity at this level corresponds to the $CO_2$ - water contact (CWC). The 3D form of the fluid contact at the base of the topmost layer was constructed by fitting a smooth subhorizontal surface through the elevations of the CWC (note this surface is not truly horizontal because it is constructed in two-way time, not depth and also because of significant fluid dynamic effects – see below). The two-way time thickness of the topmost layer was then calculated by subtracting the elevations of the reservoir top from the corresponding elevations of the CWC. These were then converted to true (depth) thicknesses (Fig. 8) using a simple velocity model for the overburden, based on well velocity data. Finally, as above, layer saturations were calculated (Equation 1).

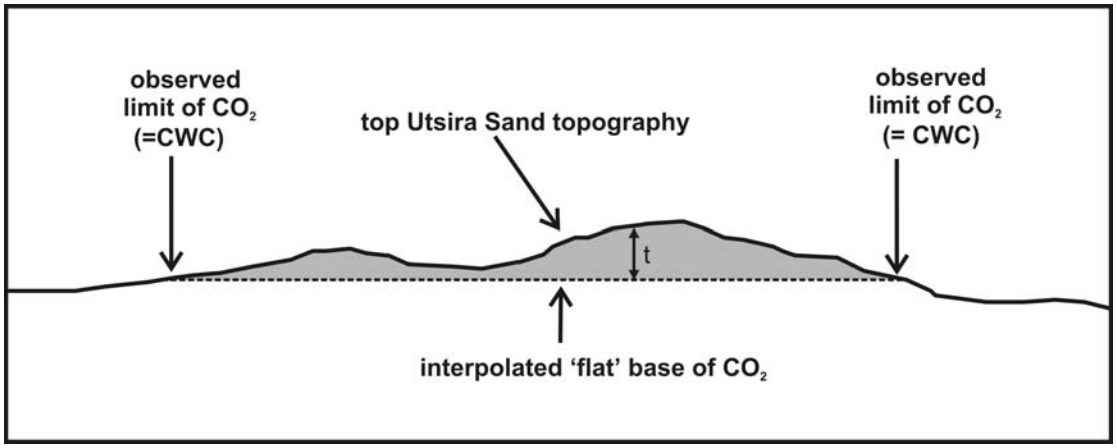


***Figure 7*** *Schematic cross-section through the topmost $CO_2$ layer, showing top reservoir topography and a nominally flat $CO_2$ – water contact. Thickness of the $CO_2$ layer (t) is the difference in elevation between the top reservoir and the CWC.*

Evaluation of the thickness maps produced by the two methods shows that structurally-derived layer thicknesses have a clear correlation with layer reflectivity (Fig. 3), supporting the general assumption of thin layer tuning. However it is also clear that the structurally-derived thicknesses are in places significantly larger than the thicknesses derived from reflectivity. The main reason for this is probably the non-linearity of the amplitude-thickness relationship whereby amplitude change is quite small for layer thicknesses above about 5 m (Fig. 5a). Application of the tuning assumption will generally tend to progressively underestimate layer thicknesses around and above the tuning thickness. Other uncertainties in the reflectivity-derived thicknesses include estimation of the maximum tuning amplitude and also the layer velocity. The structurally-derived thicknesses are therefore considered to be generally the more reliable. On the other hand, it is clear that layer reflectivity extends into localized areas where the structurally-derived layer does not, for example in the southern part of the layer (compare Figures 6 and 8). This is because the structural analysis does not allow $CO_2$ to be present wherever the constructed CWC is shallower than the topseal (Figure 7). In reality the $CO_2$ layer is a dynamic entity with significant horizontal flow and perhaps supplied from below by a number of feeders, some of which may lie beneath topographic depressions in the topseal. These processes will lead to general layer thickening and allow locally 'overdeepened' areas of caprock topography to be underlain by $CO_2$.

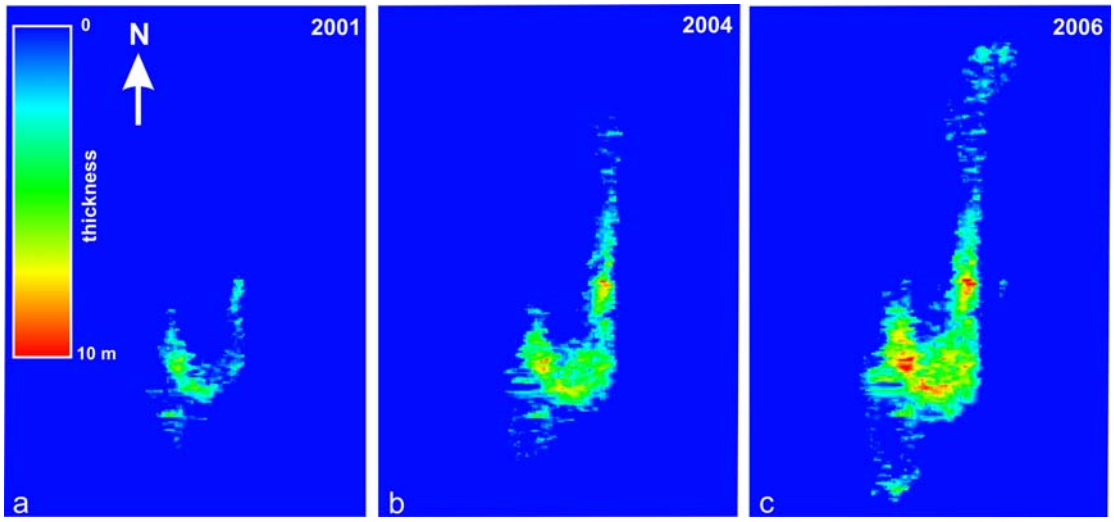


***Figure 8*** *Topmost $CO_2$ layer thicknesses derived from structural analysis.*

The volume of $CO_2$ within the topmost layer was computed for the two methods of thickness determination using calculated average saturations and an assumed mean sand porosity of 0.38 (Table 1). As discussed above, volumes derived from the structural analysis are rather higher than those derived from the reflectivity, and, overall are considered to be more reliable.

| Date | Volume from amplitudes ($m^3$) | Volume from structural analysis ($m^3$) |
|---|---|---|
| 1999 | very small | very small |
| 2002 | 66684 | 107380 |
| 2004 | 320219 | 429341 |
| 2006 | 615876 | 805409 |

***Table 1*** *Observed volumes of $CO_2$ in the topmost layer computed from the two different methods.*

From the topmost layer volumes, the rate at which $CO_2$ has arrived at the top of the reservoir can be estimated, bearing in mind that $CO_2$ first arrived at the reservoir top in 1999, just prior to the first seismic repeat survey when just two small patches of $CO_2$ had accumulated (Fig. 4a). Taking the structurally-derived volumes, an estimated $1.07 \times 10^5$ $m^3$ of $CO_2$ had arrived at the reservoir top between 1999 and the time of the 2001 survey, an average flux of ~135 $m^3$ per day. Between the 2001 and 2004 surveys ~$3.22 \times 10^5$ $m^3$ of $CO_2$ arrived at the reservoir top, an average flux of ~ 316 $m^3$ $day^{-1}$. Between the 2004 and 2006 surveys a further ~$3.76 \times 10^5$ $m^3$ of $CO_2$ arrived at the reservoir top, averaging ~540 $m^3$ per day. This marked increase in flux arriving at the reservoir top occurred despite a relatively uniform rate of $CO_2$ input at the injection point.

**Numerical flow simulation of the whole plume flux**

A simple TOUGH2 flow model was set up to simulate the observed growth of the $CO_2$ plume (Fig. 9). Modelled reservoir geometry was axisymmetric (radial), with a flat reservoir top and horizontal intra-reservoir mudstones. The latter were all 1m thick except for the uppermost, which was 5 m thick (Fig. 1b). These deliberately minimal assumptions are justified by the lack of detailed information on internal reservoir structure.

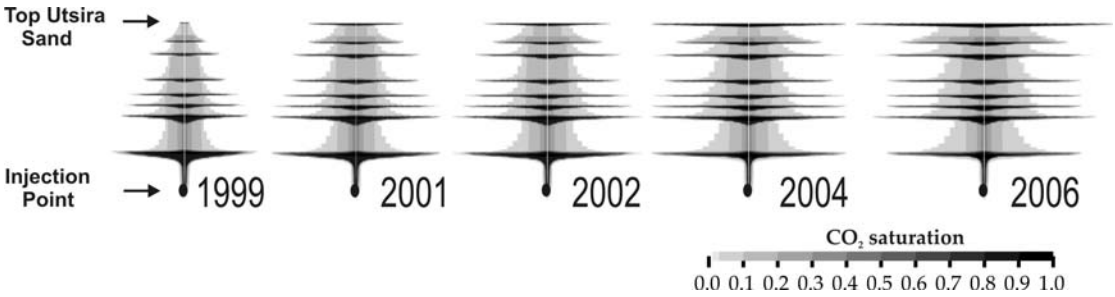


***Figure 9*** *Simulated growth of the $CO_2$ plume from 1999 to 2006 from the TOUGH2 axisymmetric flow model.*

The vertical spacing of the mudstones was set to match the relative spacing of the seismic reflections (Fig. 2). The temperature of the reservoir top was set at 29°C and the injection point at 36°C, values in line with available information (see discussion below). Sand properties were based on laboratory core measurements. Mudstones were assumed to be uniformly semi-permeable with relative permeability to $CO_2$ increasing with $CO_2$ saturation. The flow properties of the mudstones, permeability and capillary entry pressure (Table 2), are the dominant factors in determining the rate of upward migration through the reservoir, and were adjusted such that the simulation matched the observed arrival of $CO_2$ at the top of the reservoir in 1999. This occurred just prior to the first repeat survey (Fig. 4a) and is a very well-constrained key calibrating observation.

| | Intra-reservoir mudstones in TOUGH2 model | Laboratory caprock core |
|---|---|---|
| Capillary entry pressure (Pa) | $1.6 \times 10^{4}$ | $1.6 – 1.9 \times 10^{6}$ |
| Permeability ($m^2$) | $9 \times 10^{-14}$ | $4 \times 10^{-19}$ |

***Table 2*** *Flow properties of intra-reservoir mudstones in the flow model, compared with core measurements from caprock ($0.9869 \times 10^{12}$ $m^2$ equates to 1 Darcy).*

The flow simulation (Fig. 9) reproduces the key properties of the $CO_2$ plume, in particular the characteristic tiered 'christmas-tree' profile caused by the accumulation of thin layers of $CO_2$ spreading laterally beneath each intra-reservoir mudstone. It also predicts that the uppermost $CO_2$ layer shows very rapid lateral spread (Fig. 9). This is driven by a progressive increase in the modelled rate of $CO_2$ arriving at the topmost layer from 1999 onwards (Fig. 10). This is despite the relatively uniform $CO_2$ input at the injection point and is due largely to increased effective permeabilities within the central part of the plume as the intra-reservoir mudstones become progressively more saturated with $CO_2$ and relative permeability to $CO_2$ increases.

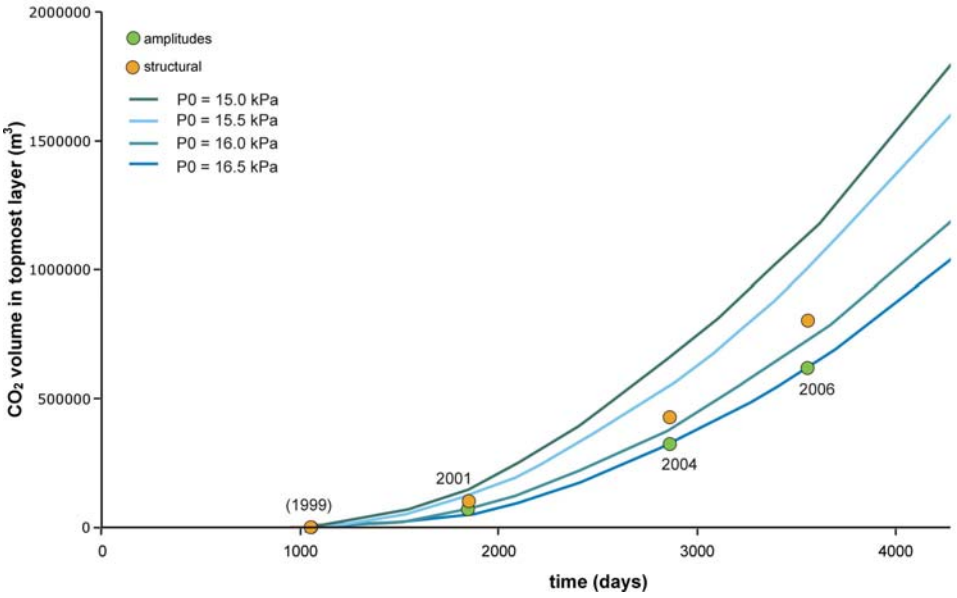


***Figure 10*** *Growth of the topmost $CO_2$ layer. Green and orange circles denote observed volumes derived from the seismic amplitudes and from structural analyis of the CWC respectively (Table 1). Solid lines show TOUGH2 flow simulation with semi-permeable intra-reservoir mudstones and a range of capillary entry pressure.*

Fluxes predicted by the flow simulation are, therefore, consistent with observed fluxes derived from the seismic data, showing a steady increase in the rate of $CO_2$ flowing into the topmost layer. The simulation, however, assumes Darcy flow through semi-permeable intra-reservoir mudstones with capillary entry pressures much lower than measured values from the caprock (Table 2), which laboratory testing shows to be a capillary seal (Harrington et al. in press). These modified values are required for the $CO_2$ to reach the top of the reservoir in the observed timespan (immediately prior to the 1999 survey). Even allowing for the simplified geometry of the axisymmetric model, this is paradoxical, because the well logs (Fig. 1b) suggest that the thin mudstones are lithologically similar to the caprock and would, at least when intact, form capillary seals. It seems likely therefore that $CO_2$ migration through these mudstones is actually not by Darcy flow but via some form of pathway flow, the pathways becoming more effective, or more numerous with time. This is also consistent with measured pressure distributions in laboratory samples during long-term flow testing, which suggest pathway rather than Darcy flow (Harrington et al. in press). The nature of these pathways is uncertain however. Small faults have been identified in the Utsira Sand, probably related to differential compaction during burial. More radically, Hermanrud et al. (2007) have suggested that fluidisation effects within the main feeder chimney may have induced minor collapse and faulting of the layers within the reservoir. Whether natural or induced, small faults displacing the intra-reservoir mudstones seem to be the likeliest candidates for providing the permeability enhancement required to explain the observed upward flow. A number of alternative explanations may be considered. Zweigel et al. (2004) showed that most of the individual intra-reservoir mudstones are not correlatable from well to well, indicating lateral impersistence and/or the presence of ‘holes’. Holes in the mudstones could be due to erosive removal, possibly by channelling, or soft

sedimentary processes such as sand mobilisation. Alternatively, geochemical processes may play a part. In the short-term, evaporation of residual water into the $CO_2$ could cause dehydration and possible shrinkage of the mudstones. Mineralogical changes are thought unlikely to occur significantly in the short timescales considered here. Moreover experimental work on the reactivity of $CO_2$ - caprock systems at reservoir conditions (summarised in Chadwick et al. 2008) indicates that mineralogical changes would tend to reduce porosity (and by implication permeability) in mudstone lithologies. Finally, recent experimental work has suggested that in $CO_2$ – water systems in argillaceous rocks (i.e. sealing strata), $CO_2$ may show intermediate wetting properties, thereby reducing capillary entry pressures to $CO_2$ (e.g. Chiquet et al. 2005). However, by itself this process cannot explain the observed rate of migration of $CO_2$ to the top of the reservoir because the intrinsic permeability of the mudstones is still much too low.

## Detailed history-matching of the topmost layer spreading

The growth of the topmost layer between 1999 and 2006 is quite striking (Fig. 4), and has involved rapid lateral spreading of free $CO_2$ controlled by top reservoir topography. The $CO_2$ initially impacted the topseal within a local topographic dome, then spilled northwards along a prominent north-trending linear ridge before entering a more vaguely defined northerly topographic high (Fig. 3). Lateral migration was particularly rapid along the linear ridge where the $CO_2$ front advanced northwards at about one metre per day between 2001 and 2004. In order to examine layer evolution more closely, a 3D flow model was set up. The top reservoir surface was mapped from the baseline (1994) seismic dataset and depth-converted using a layer-cake, laterally uniform velocity model (available wells constrain regional velocities but are not sufficiently closely-spaced to constrain local velocity variation). The nature of the $CO_2$ supply to the topmost layer depends on the transport properties of the relatively thick (>5m) mudstone immediately beneath (Fig. 1b). As discussed above, pathway flow is considered most likely, but the number of individual pathways is uncertain. In 1999, initial development of the topmost layer was as two seemingly distinct small accumulations (Fig. 4a), of which the southerly appears to have been fed directly by the main feeder chimney (Fig. 2). The simplest interpretation of the northerly accumulation is that it was supplied laterally from the southerly one, but a second smaller feeder, supplying from directly below, cannot be ruled out. For simplicity, the flow modelling assumed a single feeder, located between the two initial accumulations, with modelled $CO_2$ flux into the layer matched to the structurally-derived volumes (Table 1). A minor adjustment to the model was also made to allow for the fact that the $CO_2$ injected at Sleipner contains up to about 2% methane, lowering density and increasing buoyancy. The TOUGH2 version used for modelling does not have an option for $CO_2$/methane mixtures, so to account for this, the top reservoir temperature in the model was raised to 31.5 °C, giving a pure $CO_2$ density comparable with that of a $CO_2$ – methane (2%) mixture at 29°C.

### *Permeability effects*

Permeability values for the Utsira Sand range from laboratory determinations of 2 – 3 Darcy (with no evidence of horizontal/vertical anisotropy), to more regional estimates of up to 8 Darcy from large-scale water production (Zweigel et al 2004).

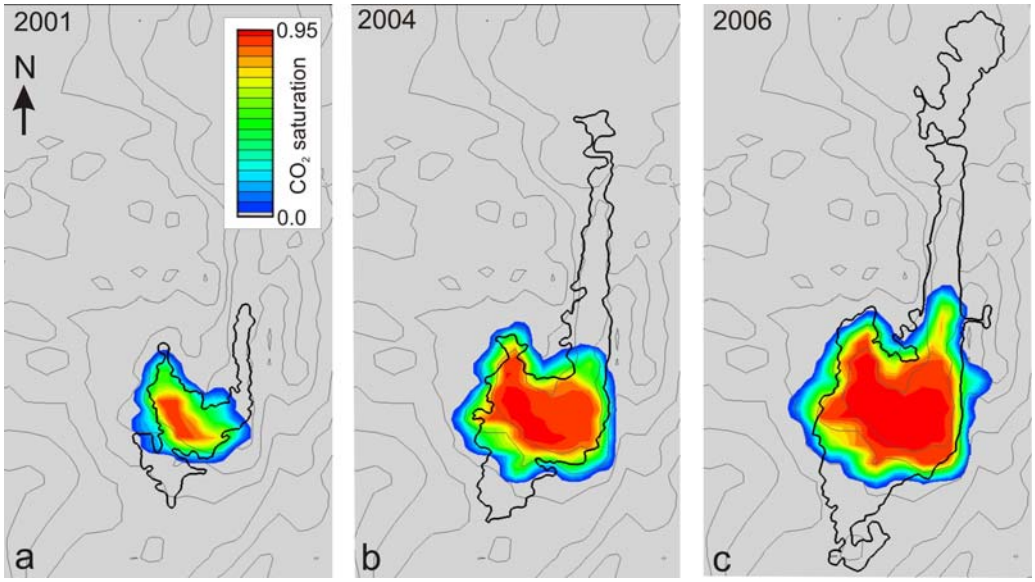


***Figure 11*** *Modelling topmost layer spreading from 2001 to 2006 assuming a reservoir permeability of 3 Darcy. Polygons denote observed $CO_2$-water contacts.*

An initial flow simulation was run using an isotropic reservoir permeability of 3 Darcy (Fig. 11), in accordance with the core measurements. The spread and lateral migration of the simulated layer is much slower than that of the real layer, the modelled $CO_2$ front barely reaching the southern end of the north-trending ridge. The modelled migration is also more obviously radial from the feeder point than the observed spreading, with a greater tendency to spread east-west.

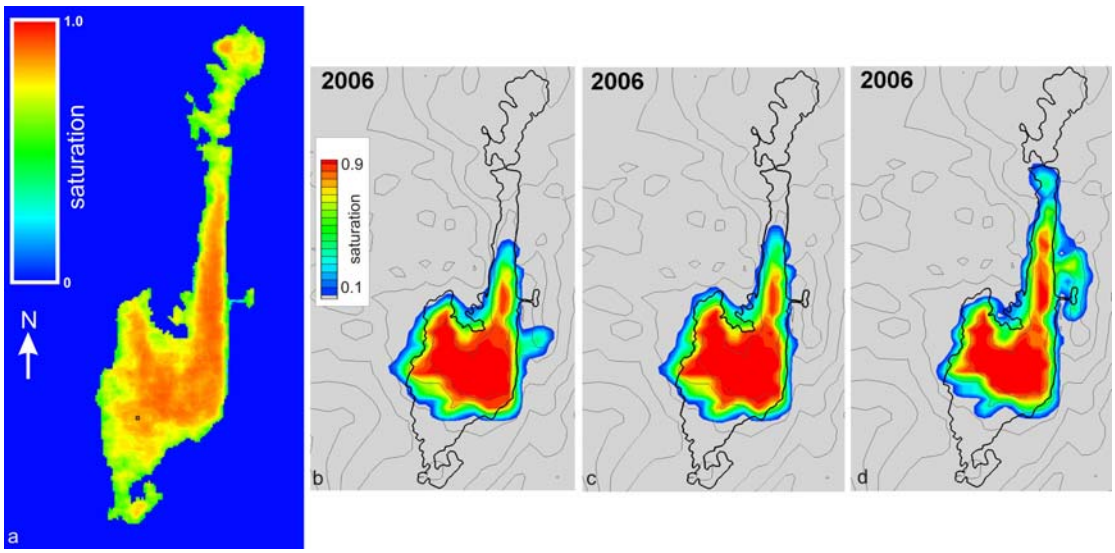


***Figure 12*** *The topmost layer in 2006. a) Observed extents b) TOUGH2 simulation with k = 6 Darcy c) TOUGH2 simulation with k = 3 Darcy E-W and 10 Darcy N-S d) TOUGH2 simulation with k = 3 Darcy E-W, 10 Darcy N-S and higher reservoir temperature.*

In order to increase the slow simulated spreading rates, a number of flow simulations were run with higher permeability values (Fig. 12). Permeabilities of 6 Darcy (Fig. 12b) and also 10 Darcy, produced more pronounced lateral spreading, but still insufficient to match the observations. The modelled migration also remains more radial about the feeder point. In order to address this, permeability anisotropy was introduced: 3 Darcy E-W and 10 Darcy N-S. Specific geological justification of this is not obvious, though the assumption is qualitatively consistent with the generally N-trending depositional geometry of the Utsira Sand (Gregerson et al. 1997). With anisotropic permeability the match is improved somewhat (Fig. 12c), but migration along the north-trending ridge is still much slower than actually observed. It is clearly difficult to match the observed spreading of the topmost layer by adjusting permeability alone. Even simulations with improbably extreme values of anisotropic permeability, 40 Darcy N-S and 10 Darcy E-W, failed to match the observed northward spreading.

***Buoyancy effects***

Lateral migration of the topmost layer is driven by buoyancy forces arising from the relatively low density of the injected $CO_2$ relative to the reservoir pore-water. To test whether enhanced buoyancy could contribute to better history-matching, the top reservoir temperature in the model was increased to 36°C, reducing the density of the $CO_2$ by about 300 $kgm^{-3}$. A simulation was then run at this higher temperature but with the same injected volumes and with 3/10 Darcy anisotropic permeabilities (Fig. 12d). This simulation shows a better match than the lower temperature models but still fails to reproduce both the northward and southward extents of the observed layer. The justification for reducing plume density via increased temperatures is in any case questionable. The reservoir temperature at Sleipner is believed to be well constrained: a temperature measurement from one of the Sleipner wells has been recently confirmed by downhole measurements from the nearby Volve Field where water is being produced from the Utsira Sand (Ola Eiken pers. comm.). Nevertheless some doubt remains: interpolation between the seabed and measured temperatures in the much deeper Sleipner East gasfield (Christian Hermanrud pers. comm.) would suggest temperatures in the Utsira Sand up to a few degrees higher than the measured values.

***Topographic effects***

It is clear that neither adjusting reservoir permeability nor injected fluid buoyancy can satisfactorily match the simulations with the observed spread of the topmost $CO_2$ layer, in terms of either its northerly or southerly extents. The lack of southerly spreading can partly be explained by the model simplification of a single $CO_2$ feeder located between the two 1999 patches. Placing a feeder directly beneath the southerly patch would produce much more southward spread. Additional feeders to the south may also be developing as the layer grows. The lack of northward spread in the model is more problematical. Additional feeders beneath the N-S trending tongue of $CO_2$ can probably be discounted due to the lack of a $CO_2$ source layer beneath. In addition, specific details of migration which also do not match the observations, such as the simulated spillage eastward from the north-trending linear ridge (Fig. 12d), require explanation. It is likely that slight inaccuracies in the depth topography of the top reservoir surface may explain these discrepancies.

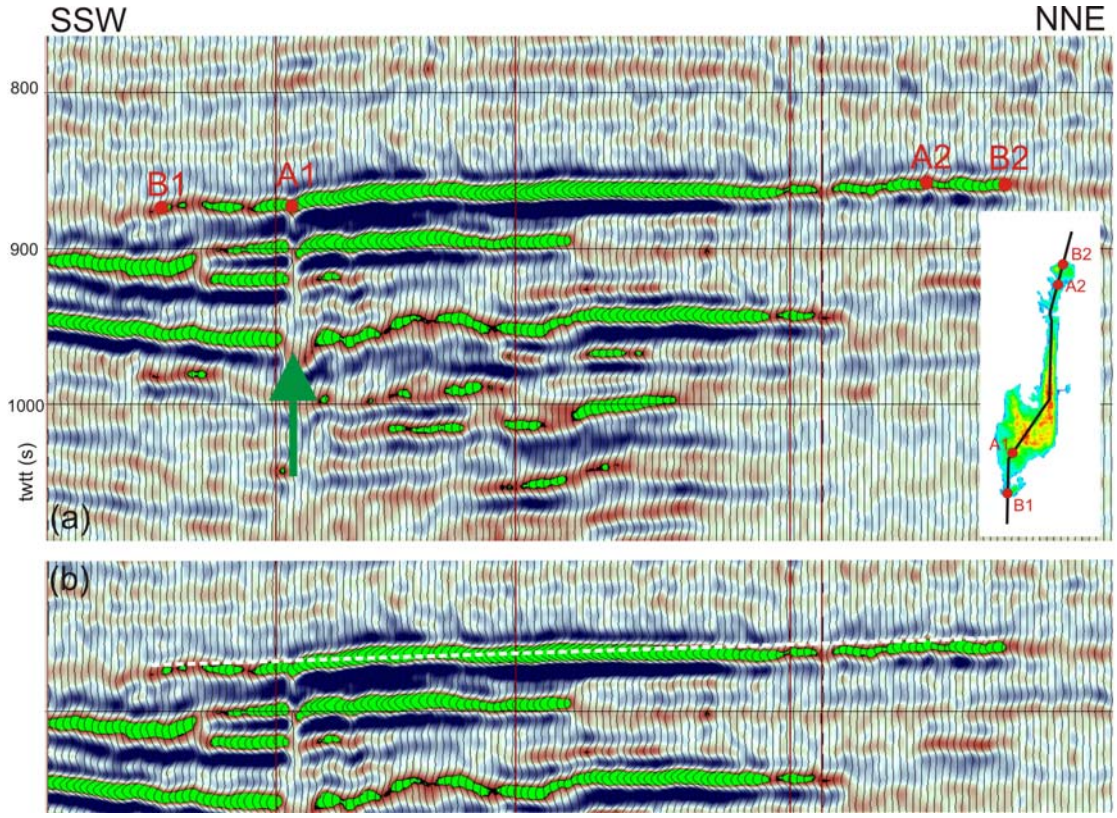


***Figure 13*** *Seismic line through the $CO_2$ plume. a) Detailed geometry of the topmost layer in two-way travel-time. The main feeder chimney (arrowed) supplies the layer at point A1. b) Deviation of the topmost layer from planar geometry (white dots). Reflective $CO_2$ layers in green.*

A detailed cross-section through the topmost layer (Fig. 13a) shows that its observed northward progression involved rapid migration along an apparently near-horizontal ridge crest. Top reservoir depths were calculated using a laterally uniform 'layer-cake' overburden velocity model based on average velocities from a number of wells in the vicinity; depths are, in consequence, a simple transform of seismic two-way travel-time. Apparently paradoxical migration trends could therefore be explained by errors in the topography of the topseal produced by lateral velocity variations which have not been accounted for in the depth-conversion.

An initial test of this hypothesis is to examine the overall dip of the topseal. The feeder chimney impacts the topseal at point A1 at a two-way travel-time of 873 ms (Fig. 13). A local topographic culmination north of the linear ridge, point A2, lies at a two-way travel-time of 856 ms. The travel-time difference between A1 and A2 converts to a depth difference of 18.5 m, which over a horizontal spacing of 2249 m gives an average gradient of 0.0082. A more conservative estimate of topseal dip may be obtained by comparing the relative elevations of the southernmost and northernmost extremities of the layer, points B1 and B2 respectively. These two points have an elevation difference of 17.4 metres over a distance of 2895 m, giving an average gradient of 0.0058.

In order to test potential $CO_2$ migration rates along dips of this order, a simple synthetic surface model was constructed. This has two circular domes whose relief

and separation matches the observed topseal surface, joined by a linear ridge of similar geometry to that observed. Two surface options were examined, one with a uniform gradient along the ridge of 0.0058 and one with a gradient of 0.0082 (Fig. 14).

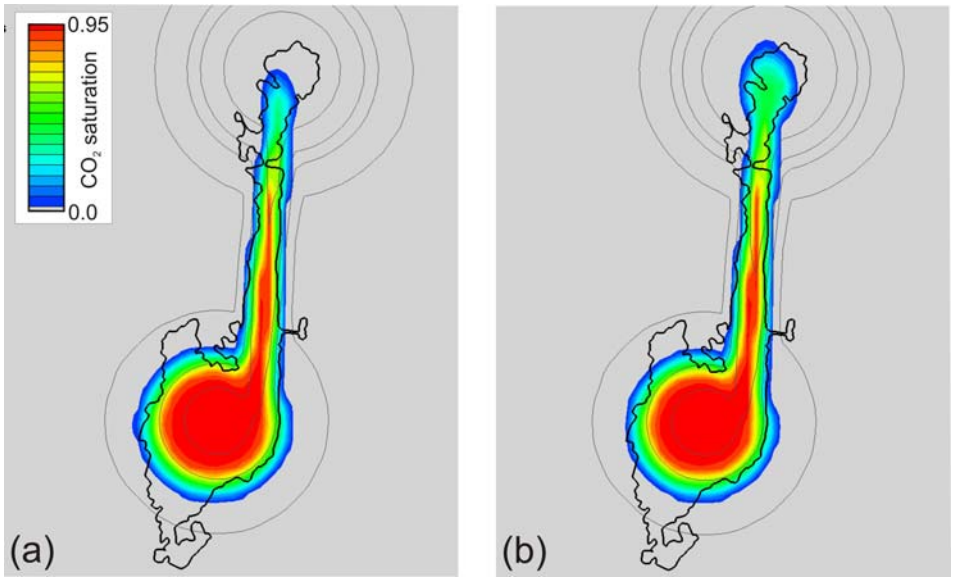


***Figure 14*** *Flow simulation of synthetic surface with sand permeability of 10 Darcy a) average gradient of 0.0058 b) average gradient of 0.0082.*

The simulations show that a synthetic surface with a smooth, uninterrupted, dip in the observed range can produce the required rate of lateral migration, albeit requiring a high modelled permeability. A key property of the synthetic surface is that a uniform dip is maintained along the linear ridge. Close inspection of the real data (Fig. 13b) show local perturbations of up to 5 ms two-way travel-time along the ridge with respect to a uniform gradient. The downwarp towards the northern end of the ridge effectively retards northward migration of the $CO_2$ in the flow simulations. If however this downwarp were not real, but just a localised time-shift (pushdown) due to lateral velocity variation, then the discrepancy between the observed and simulated migration patterns could be explained.

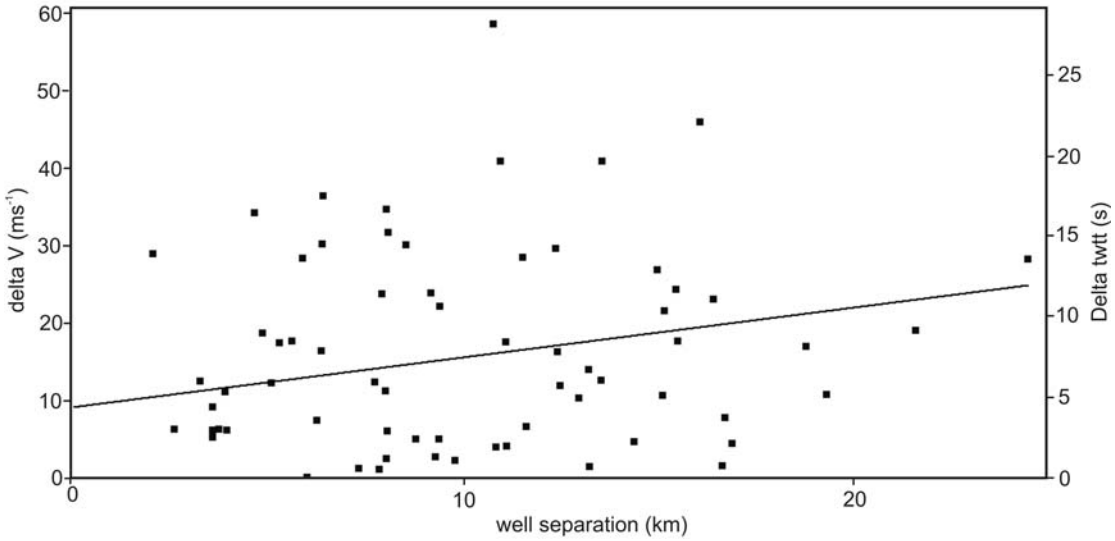


***Figure 15*** *Average velocity variation to top Utsira Sand showing velocity difference between pairs of wells and corresponding time-shifts. Linear best fit also shown.*

There are a number of wells in the vicinity with velocity data, but these are too spatially scattered (typically more than 2 km apart), to explicitly map local velocity variations. Average velocities to the top of the Utsira Sand were calculated for these wells. Well pairs were selected, their spacing noted, and the difference in velocity between them calculated. Velocity difference against well spacing was then plotted for all well pairs (Fig. 15). Significant velocity variation is evident, with differences up to more than 50 $ms^{-1}$, but these are not clearly related to well spacing with velocity differences up to 30 $ms^{-1}$ between wells only 2 to 3 km apart. This suggests that the velocity field is characterised by rapid local velocity changes which are not being properly spatially sampled by the widely-spaced wells. Velocity difference is readily converted to two-way travel-time difference. Two-way travel-time differences of 10 ms or so are common at well spacings of 2 to 3 km. The linear best fit, albeit very poorly-correlated, suggests that similar time differences could well occur over even smaller distances. It is clear therefore that the postulated time-shifts noted on the cross-section (Fig. 13b) - up to 5 ms over a distances of about one km - are fully compatible with observed velocity changes in the wells.

Accurate mapping of local velocity variation is required to resolve this issue but this is not possible with the widely-spaced well data. Seismic stacking velocities are currently being assessed, but do not appear to be sufficiently precise. Another possibility is interpretive use of the seismic data itself. Bright-spots in the overburden are clustered at certain stratigraphical levels and are probably related to accumulations of shallow gas which would lower seismic velocity. By mapping integrated bright-spot amplitudes it may be possible to scale these to relative velocity-induced time-shifts. This is currently under investigation.

To summarise, the well data show that local velocity variations are present which induce significant localised time-shifts. Time-shift corrections applied to the topseal surface prior to depth conversion could produce a smoother depth surface which

would allow simulated layer spreading to more closely match the observed data. Explicit mapping of these time-shifts has not currently been achieved however.

***Topseal properties***

The flow simulations have all assumed an impermeable reservoir topseal. This is consistent with laboratory testing on caprock core samples which measured capillary entry pressures of around 2 MPa, considerably higher than any credible reservoir pressure increase. However, although they seem to have similar geophysical log properties to the caprock, the thin intra-reservoir mudstones are required to be effectively semi-permeable for the whole plume reservoir simulation to match the observed arrival of $CO_2$ at the reservoir top (Fig. 4a). The question arises therefore as to whether the basal layers of the caprock might show similar flow properties to the intra-reservoir mudstones. There is no evidence of changes in the seismic signature of the caprock that might indicate migration of $CO_2$ through the topseal, but this is subject to finite detection capability and so does not unequivocally prove seal integrity; particularly as diffuse migration into the caprock may be difficult to detect seismically.

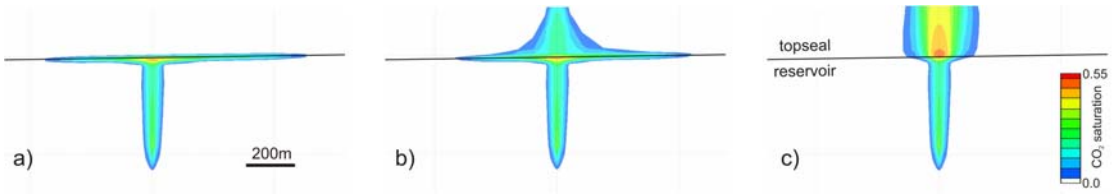


***Figure 16*** *Flow simulations (after six years) beneath a planar dipping topseal of variable flow properties a) k = 4 x $10^{-19}$ $m^2$ Pc = 2 MPa b) k = 9 x $10^{-14}$ $m^2$ Pc = 40 kPa c) k = 9 x $10^{-14}$ $m^2$ Pc = 17 kPa. Note figure has vertical exaggeration.*

In order to investigate this, a simple 3D flow model was set up, with a planar dipping topseal of gradient 0.0082 (comparable to the real dips discussed above) and a reservoir permeability of 3 Darcy. $CO_2$ was input beneath the topseal, at the volumes calculated above, for a range of topseal flow properties and the simulation run for six years (Fig. 16). With topseal properties identical to the core measurements (Harrington et al. in press) the $CO_2$ migrates up-dip more than 600 m (Fig. 16a). Modifying the topseal permeability to the modelled permeability of the intra-reservoir mudstones, but maintaining a higher capillary entry pressure allows limited migration into the caprock and reduces the up-dip migration to about 550 m (Fig. 16b). With topseal flow properties set identical to the modelled properties of the intra-reservoir mudstones (Fig. 16c) there is major ingress into the topseal with negligible up-dip migration. It is clear that migration into the caprock significantly retards lateral migration, and would not be consistent with the observed very rapid lateral migration of the topmost layer. The high observed migration rates, and the very high reservoir permeabilities that are required to simulate these, suggest therefore that the topseal is behaving as a very ‘hard’ flow barrier without exerting negligible ‘drag’ on the flowing layer beneath.

## Discussion

The type of analysis described above provides an interesting pointer to how the regulatory requirements of future large-scale underground storage may be addressed. For example, the European Storage Directive has three key requirements which have to be satisfied before liability for the storage site can revert to the licensing authority:

- Actual behaviour of the injected $CO_2$ conforms with the modelled behaviour
- There is no detectable leakage
- The storage site is evolving towards a situation of long-term stability

Because the topmost $CO_2$ layer represents the ultimate trapping level for mobile free $CO_2$ in the reservoir, understanding its behaviour is key to demonstrating both conformance and constraining future plume behaviour. Results so far suggest that the main processes governing lateral spreading of the topmost layer are quite well understood and its actual behaviour conforms reasonably well with the modelling. Regarding leakage detection, the lack of seismic changes in the caprock, together with the apparent lack of fluid transport into the caprock as deduced above, together make a strong case for no leakage. The third requirement clearly will involve much longer-term predictive modelling than the short-term history matching described here, nevertheless the latter does provide an essential stating point on which to base longer-term prediction.

## Conclusions

The topmost $CO_2$ layer in the Sleipner plume represents the ultimate trapping level for mobile free $CO_2$ in the reservoir. As such it can provide useful insights into key elements of reservoir performance, both in the short and longer term.

Volumetric analysis of the layer closely constrains total upward $CO_2$ flux through the reservoir. This allows assessment of bulk reservoir flow properties and how these change with time. The thin intra-reservoir mudstones exert the main control on reservoir flow. Laboratory measurements suggest that, in intact form, these should act as capillary seals, so it is inferred that transport is via pathway flow rather than Darcy flow, possibly associated with networks of small faults or other ‘holes’ perhaps of sedimentary origin. Calculated $CO_2$ fluxes to the topmost layer have steadily increased with time, suggesting that the feeder pathways are evolving, becoming either more transmissive with time and/or increasing in number.

Detailed 3D history-matching of the topmost layer is challenging, most likely because of uncertainties in exact topseal topography. It nevertheless provides insights into the flow properties of both the topmost reservoir sand and also the integrity of the seal. High observed lateral spreading rates are consistent with very high permeabilities, possibly with some anisotropy. They also suggest that the topseal presents a very ‘hard’ flow barrier which exerts minimal ‘drag’ on the lateral flow beneath.

Studies such as this, concentrating on defining the process and performance of the storage system, within and immediately around the reservoir, can provide a robust basis for meeting the regulatory requirements for the large-scale deployment of CCS.

## Acknowledgements

We thank theCO2ReMoVe consortium for permission to publish this work. CO2ReMoVe is funded by the EU 6th Framework Programme and by industry partners BP, ConocoPhillips, ExxonMobil, Statoil, Schlumberger, Total, Vattenfall and Wintershall. R&D partners are BGR, BGS, BRGM, CMI, DNV, ECN, GFZ, GEUS, IFP, IMPERIAL, OGS, SINTEF, TNO and URS. This paper is published with permission of the Executive Director, BGS (NERC).

## References

Arts, R., Eiken, O., Chadwick, R.A., Zweigel, P., van Der Meer L. & Zinszner, B. 2003. Monitoring of $CO_2$ injected at Sleipner using time lapse seismic data. In: Gale, J. & Kaya, Y. (eds) *Greenhouse Gas Control Technologies*. Elsevier Science Ltd, Oxford, 347 – 52.

Baklid, A., Korbol, R & Owren, G. 1996. Sleipner Vest $CO_2$ disposal, $CO_2$ injection into a shallow underground aquifer. *SPE Annual Technical Conference and Exhibition*, Denver Colorado, USA, SPE Paper 36600, 1 - 9.

Chadwick, R.A., Arts, R., Eiken, O., Kirby, G.A., Lindeberg, E. & Zweigel, P. 2004. 4D seismic imaging of a $CO_2$ bubble at the Sleipner Field, central North Sea. In: Davies, R.J., Cartwright, J.A., Stewart, S.A., Lappin, M. & Underhill, J.R. (eds) *3-D Seismic Technology: Application to the Exploration of Sedimentary Basins*. Geological Society, London, Memoirs, 29, 311-320.

Chadwick, R.A. Arts, R. & Eiken, O. 2005. 4D seismic quantification of a $CO_2$ plume at Sleipner, North Sea. In: Dore, A.G., Vining, B.A. (eds). *Petroleum Geology: North-West Europe and Global Perspectives*. The Geological Society, London, 1385 – 1399.

Chadwick, R.A., Arts, R., Bernstone, C., May, F., Thibeau, S & Zweigel, P. 2008. *Best Practice for the Storage of $CO_2$ in Saline Aquifers*. British Geological Survey Occasional Publication No. 14. ISBN: 978-0-85272-610-5. 277 pp, Keyworth, Nottingham.

Chiquet, P., Broseta, D. & Thibeau, S. 2005. Capillary alteration of shaly caprocks by carbon dioxide. *Society of Petroleum Engineers Paper SPE 94183.*

Gregersen, U., Michelsen, O & Sorensen, J.C. 1997. Stratigraphy and facies distribution of the Utsira Formation and the Pliocene sequences in the northern North Sea. *Marine and Petroleum Geology*, 14, 893 – 914.

Harrington, J.F., Noy, D.J., Horseman, S.T., Birchall, D.J. & Chadwick, R.A. (in press) Laboratory study of gas and water flow in the Nordland Shale, Sleipner, North Sea. In: Grobe, M., Pashin, J. & Dodge, R. (eds) *Carbon Dioxide Sequestration in Geological Media*. Special Publication of the American Association of Petroleum Geologists.

Hermanrud, C., Zweigel, P., Eiken, O., Lippard, J. & Andresen, T. 2007. $CO_2$ flow in the Utsira Formation: inferences made from 4D seismic analysis in the Sleipner area. *European Conference of the American Association of Petroleum Geologists abstract*, Athens.

IPCC 2005. *IPCC Special Report on Carbon Dioxide Capture and Storage. Prepared by Working Group III of the Intergovernmental Panel on Climate Change.* Metz, B., Davidson, O, de Coninck, H.C, Loos, M. & Meyer, L.A. (eds). Cambridge University Press, Cambridge, United Kingdom and New York, NY, USA, 442 pp.

Lindeberg, E., Zweigel, P., Bergmo, P., Ghaderi, A. & Lothe, A. 2001. Prediction of $CO_2$ distribution pattern by geology and reservoir simulation and verified by time-lapse seismic. In: Williams, D.J., Durie, R.A., McMullen, P., Paulson, C.A.J. &

Mavko, G., Mukerji, T.. & Dvorkin, J. 2003. *The Rock Physics Handbook.* 2nd Edition. Cambridge University Press. 329pp.

Smith, A.Y. (eds) *Greenhouse Gas Control Technologies.* CSIRO Publishing, Collingwood, Australia, 372 – 377.

Zweigel, P., Arts, R., Lothe, A.E. & Lindeberg, E. 2004. Reservoir geology of the Utsira Formation at the first industrial-scale underground $CO_2$ storage site (Sleipner area, North Sea). In: Baines, S., Gale, J. & Worden, R.H. (eds) *Geological Storage for $CO_2$ Emissions Reduction*. Special Publication of the Geological Society, London, 233, 165 – 180.